11th World Congress on Computational Mechanics (WCCM XI)
5th European Conference on Computational Mechanics (ECCM V)
6th European Conference on Computational Fluid Dynamics (ECFD VI)
E. Oñate, J. Oliver and A. Huerta (Eds)

NUMERICAL INVESTIGATION ON PARTICLE RESUSPENSION IN TURBULENT DUCT FLOW VIA DNS-DEM: EFFECT OF COLLISIONS

Hao Zhang[1,2], F. Xavier Trias[1], Andrey Gorobets[1,3], Dongmin Yang[4], Assensi Oliva[1], Yuanqiang Tan[2]

[1]Heat and Mass Transfer Technological Center, Technical University of Catalonia
ETSEIAT, C/Colom 11, 08222 Terrassa, Spain
e-mail: cttc@cttc.upc.edu

[2]School of Mechanical Engineering, Xiangtan University, Hunan 411105, China

[3] Keldysh Institute of Applied Mathematics of RAS, 4A, Miusskaya Sq., Moscow, 125047, Russia

[4] School of Civil Engineering, University of Leeds, Leeds LS2 9JT, UK

Key words: Particle resuspension, Turbulent duct flow, DNS-DEM, Collisions

Abstract. Particle transportation in a fully developed turbulent duct flow is numerically investigated under the effect of wall-normal gravity force. The hydrodynamic modeling of the fluid phase is based on direct numerical simulation. The kinematics and trajectory of the particles as well as the particle-particle interaction are described by the discrete element method (DEM). By using a soft-sphere DEM where the particles and the walls are specified by material properties in the simulation, the effect of collisions on the particle resuspension rate is discussed. The collisions are found to influence on the particle resuspension rate near the duct floor whereas hardly affect the particle behavior near the duct center.

1 INTRODUCTION

Particle transportation in a fully developed turbulent duct flow is commonly encountered in both engineering and environmental applications [1]. Under the action of the wall-normal gravitational force, the particles may deposit on the duct floor. It is known that there is the secondary flow of Prandtl's second kind in turbulent duct flow [2], therefore, the depositing particles can be resuspended by this secondary motion as well as collisions between the particles and between the particles and the walls. An understanding of how these flows behave is of clear benefit to dig the mechanism of the particle-laden

turbulent duct flow and extend the lifespan of context devices.

The information provided by the experimental study [3] is very limited. Nowadays, numerical simulations are widely adopted to assist the reliable scale-up, redesign of different processes due to the fact that numerical simulations can provide various information that is extremely difficult to observe online by physical experimentation at this stage of development. The single phase turbulent duct flow have been numerically investigated in [4, 5] using direct numerical simulation (DNS) and in [6] using Large-Eddy Simulations (LES). Moreover, Yao and Fairweather [7] performed a LES coupled with a Lagrangian Particle Tracking (LES-LPT) to investigate the particle resuspension mechanism in turbulent duct flows. Then, this work was followed by Adams et al. [8] using Reynolds-averaged Navier-Stokes equations with turbulent models (RANS-LPT). However, the inter-particle collisions were neglected in [7] and [8]. Tanaka and Tsuji [9] have indicated that the effect of inter-particle collisions is important even in dilute flow. In this study, we focus on the DNS of particle-laden turbulent flows in a straight duct. The effect of collisions on the particle resuspension rate is studied with special emphasis. Here the kinematics and trajectory of the discrete particles as well as the particle-particle interaction are described by the discrete element method (DEM) [10]. The DEM has been continually adopted to investigate particulate flows [11, 12, 13] and multi-phase flows [14, 15, 16] due to its natural advantage to characterize the granular matters. In this study, the interaction in the DEM is based on the theoretical contact mechanics thereby it is possible to directly use the material properties of the particle in the calculation. A small overlap between the rigid particles is allowed to represent the physical deformation that takes place between the contacting elements.

2 MATHEMATICAL DESCRIPTIONS

2.1 Governing equations and numerical methods for DNS

We consider the simulation of incompressible turbulent flows of Newtonian fluids. Under these assumptions, the governing equations of the fluid phase read

$$\left\{ \begin{array}{rcl} \nabla \cdot u_f & = & 0 \\ \frac{\partial u_f}{\partial t} + \nabla \cdot (u_f \otimes u_f) & = & -\nabla p + \nu \nabla^2 u_f \end{array} \right. \tag{1}$$

where u_f and p represent the fluid velocity and kinematic pressure fields, respectively, and ν is the kinematic viscosity. The incompressible NS equations (2) are discretized on a staggered Cartesian grid using a symmetry-preserving discretization [17]. For the temporal discretization, a second-order explicit one-leg scheme is used for both the convective and diffusive terms, the timestep is determined by a two-step linear explicit scheme on a fractional-step method proposed by Trias and Lehmkuhl [18]. For details about the numerical algorithms and the verification of the DNS code the reader is referred to [19].

2.2 Modeling of the particle-particle and particle-fluid interactions

When the particles collide directly with other particles or the walls, the DEM [10] is employed to calculate the collision force. The dynamic equations of a particle can be expressed as:

$$\begin{cases} m\frac{\partial^2 S}{\partial t^2} &= m\left(1-\frac{\rho_f}{\rho_p}\right)g + F_c + F_{fpi} \\ I\frac{\partial^2 \theta}{\partial t^2} &= \tau \end{cases} \tag{2}$$

where m and I are the mass and the moment of inertia of the particle, respectively. S is the particle position and θ is the angular position. ρ_f and ρ_p are the densities of the fluid and particle, respectively. g is the gravitational acceleration and τ is the torque. F_c and F_{fpi} are the collision force and the fluid-particle interaction force, respectively. In this study, the particles and walls are directly specified by material properties in the simulation such as density, Young's modulus and friction coefficient. When the collisions take place, the theory of Hertz [20] is used for modeling the force-displacement relationship while the theory of Mindlin and Deresiewicz [21] is employed for the tangential force-displacement calculations. For details about the theoretical illustration of the interaction law, the readers are also referred to our previous study [22].

The fluid-particle interaction force F_{fpi} is constituted by the Stokes drag force and the lift force that are related to the relative velocity between the fluid and particle, $U_r = u_f - u_p$,

$$F_{fpi} = 0.5\rho_f A_p C_D |U_r| U_r + 1.615 m_p d_p \rho_f \nu Re_s^{0.5} c_{ls} \frac{U_r \times \omega}{|\omega|} \tag{3}$$

where A_p is the cross-sectional area of the particle which is given as $A_p = 0.25\pi d_p^2$, d_p is the diameter of the particle. $C_D = 24(1+0.15Re_p^{0.687})/Re_p$ is the drag coefficient. The particle Reynolds number $Re_p = |U_r|d_p/\nu$. $Re_s = \rho_p d_p^2 |\omega|/(\rho_f \nu)$ is the particle Reynolds number of the shear flow in which $\omega = \nabla \times U_r$ stands for the fluid rotation. When $Re_p > 40$, $c_{ls} = 0.0524(\beta Re_p)^{0.5}$. When $Re_p \leq 40$, $c_{ls} = (1 - 0.3314\beta^{0.5})e^{-Re_p/10} + 0.3314\beta^{0.5}$. Here, β is a parameter given by $\beta = 0.5Re_s/Re_p$ (for $0.005 < \beta < 0.4$).

3 RESULTS AND DISCUSSION

The configuration of interest in this study is a straight duct with square section. The computational domain is $4\pi h \times h \times h$ in the streamwise and wall-normal directions, $h = 0.02m$. The Reynolds number based on the friction velocity, u_τ, the hydraulic diameter, h and the kinematic viscosity ν is $Re_\tau = hu_\tau/\nu = 300$. Periodic boundary conditions are applied in the streamwise direction. The carrier fluid is water with the density $\rho_f = 1000kg/m^3$ and the kinematic viscosity $\nu = 1.004 \times 10^{-6} m^2 s^{-1}$. The flow is driven by means of a constant pressure gradient in the streamwise direction. No-slip boundary conditions are imposed at the walls. The direction of the gravitational action is set along

$z-$direction downwards. The computational domain is covered a $322 \times 202 \times 202$ uniform staggered mesh, by doing so, the grid point closest to the sidewalls is at $\Delta y^+_{min} = 0.75$. Therefore, the grid resolution is fine enough to resolve all the relevant turbulent scales.

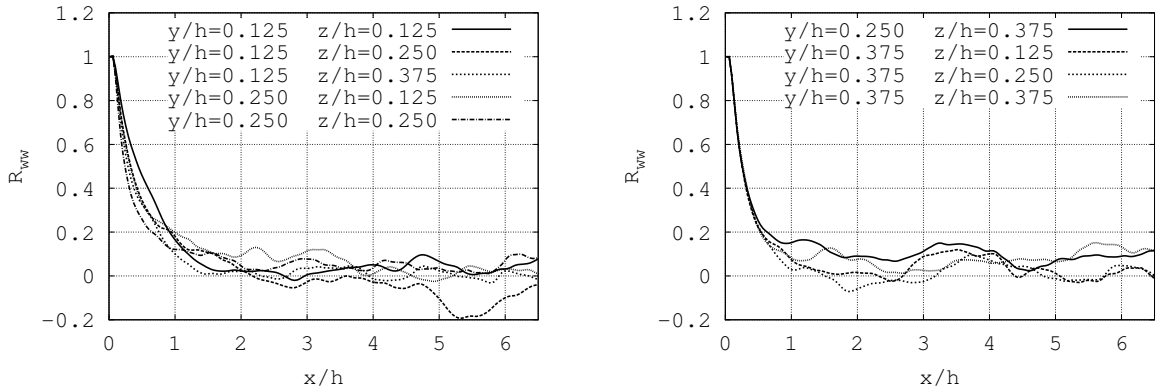

Figure 1: Two-point correlations at nine monitoring locations.

A sufficient length in the periodic $x-$direction is required to ensure that the two-point streamwise correlations of the velocity decay sufficiently for separations equal to half the streamwise length. This issue has been fully discussed in [4], however a long length ($10\pi h$) was employed by the author for safety. Based on the research of Uhlmann et al. [23], the minimum value for the streamwise period of the computational domain measures is around 190 wall units and roughly independently of the Reynolds number. In this study, the streamwise two-point correlations, $R_{\phi\phi}(\Delta x, y, z) = \frac{<\phi'(x,y,z)\phi'(x+\Delta x,y,z)>}{<\phi'^2(x,y,z)>}$, at different $(y, z)-$locations have been used to check the suitability of the numerical simulation parameters in the x-direction, where $< \cdot >$ represent the average over time. In Fig. 1, two-point correlations of the velocity component, R_{ww}, at nine different $(y, z)-$locations are shown. In all the cases, the correlation values fall to zero for separations lower than one half-period. Therefore, the computational domain in the streamwise direction is sufficiently large. From Fig. 1 it also shows the possibility to use a shorter streamwise length like $2\pi h$ in [24]. However, any cut on the streamwise length leads to a marked increase on the statistics period.

Fig. 2 displays the quadrant-averaged $v - w$ velocity vectors in the cross-section of the duct. As expected there are four pairs of counter-rotating vortexes with a symmetrical distribution. The velocity vectors are from the core to the corners which deliver fluid momentum. When approaching the corners, the fluid turns half a right-angle then flows along the wall until encounters another flow from the other corner, they flow back into the duct center together.

The above fully developed turbulent flow is used as an initial condition for the multiphase flow simulation, 20000 particles of 50 μm are randomly placed in the fully developed

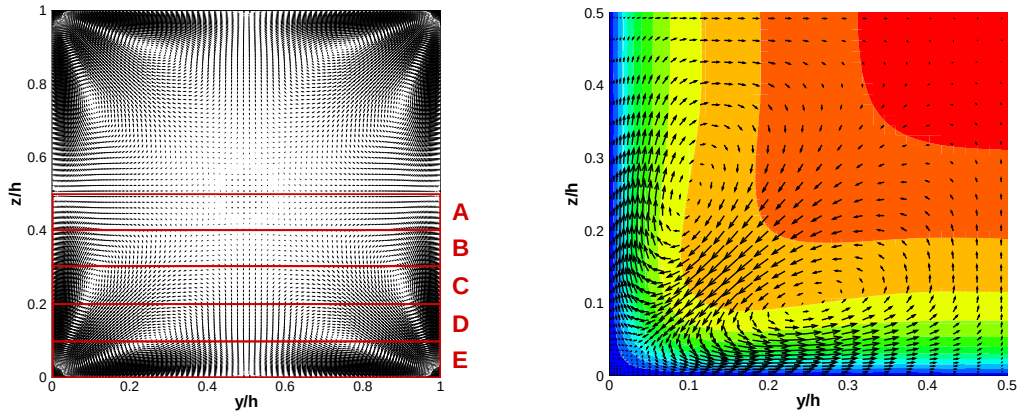

Figure 2: (a) Mean secondary flows in $y-$ and $z-$directions. (b) The zoomed view in the first quadrant with the contours for the mean streamwise velocity component

turbulent flow field. The properties of the particles are given in Table. 1 in which the dimensional and non-dimensional particle relaxation time are defined as $\tau_p = \rho_p d_p^2/(18\rho_f \nu)$ and $St = \tau_p u_\tau^2/\nu$, respectively. Numerical simulations are carried out with and without collisions, respectively. Fig. 3 displays the snapshot of the particle and velocity distributions in the duct with collisions. For the sake of clarity, only 20% of the particles are shown without changing the main trend of the distribution characteristic. It is shown that the instantaneous particle distribution is obviously influenced by the secondary flows that lead to a progressive segregation of the particles within the upper half of the duct and accumulation within the lower half.

d_p	d_p^+	E_i	ρ_p	ν_i	τ_p	St
(μm)	(-)	$(GPa\ )$	$(kg \cdot m^{-3}\ )$	(-)	$(s\ )$	(-)
50	0.75	68.95	2500	0.33	3.46×10^{-4}	0.078

Table 1: Parameters of the particles used in the simulations.

The lower half of the duct is separated into 50 squares, namely five partitions in the $z-$direction and ten partitions in the $y-$direction, each region in the $z-$direction containing ten squares is marked by A, B, C, D, E as shown in Fig. 2. The resuspension rate is defined as the ratio of the number of resuspended particles to the total number of particles within each square. Fig. 4 shows the resuspension rate with and without collisions where the solid lines stand for the resuspension rate with collisions while the dashed lines stand for those without collisions. From left to right, it is shown that the resuspension rate without collisions decreases with the height in duct which agrees with the strength of the secondary flows at different heights, the resuspension rate with collisions is a little

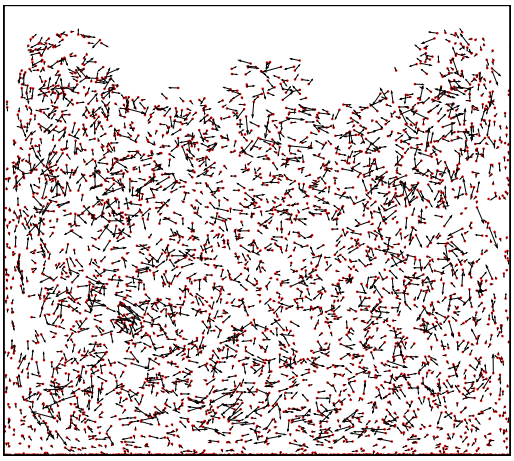

Figure 3: 2D snapshots of particle distribution with velocity vectors at $t = 12s$. Red point for the particle, black arrow for the velocity.

bit lower than that without collisions in Region A and B. However, the resuspension rate with collisions is higher than that without collisions in Regions C, D and E.

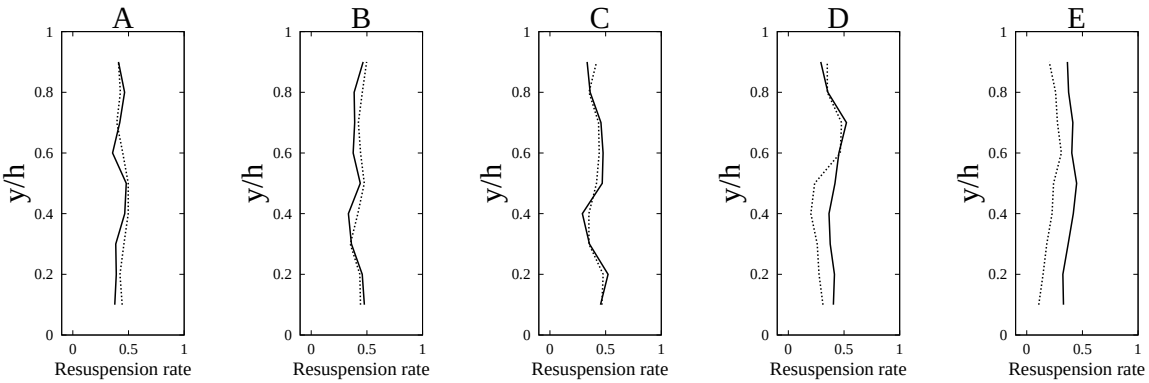

Figure 4: Particle resuspension rate in the $z-$direction for 50 μm particles. Solid line: with collisions. Dashed line: without collisions.

4 CONCLUSIONS

In this paper, the effect of collisions particle resuspension in turbulent duct flow has been numerically investigated via DNS-DEM, the effect of the inter-particle collisions on the particle suspension rate has been discussed. According to the results of the analysis, the following conclusions can be made.

- In the inner regions, the inter-particle collisions increase the deposition rates of the particles.

- In the region near the duct floor, the particle resuspension rates are significantly enhanced by the collisions.

ACKNOWLEDGMENTS

This work has been financially supported by the *Ministerio de Ciencia e Innovación*, Spain (ENE2010-17801). Hao Zhang would like to acknowledge the FI-AGAUR doctorate scolarship granted by the Secretaria d'Universitats i Recerca (SUR) del Departament d'Economia i Coneixement (ECO) de la Generalitat de Catalunya, and by the European Social Fund. F. Xavier Trias would like to thank the financial support by the *Ramón y Cajal* postdoctoral contracts (RYC-2012- 11996) by the *Ministerio de Ciencia e Innovación*. Calculations have been performed on the IBM MareNostrum supercomputer at the Barcelona Supercomputing Center. The authors thankfully acknowledge these institutions.

REFERENCES

[1] Fairweather, M. and Yao, J. *AIChE Journal* **55**(7), 1667–1679 (2009).

[2] Nikuradse, J. *Ph.D. Thesis, Gottingen. VDI Forsch* **281** (1926).

[3] Wang, S., Zhao, B., Zhou, B., and Tan, Z. *Building and Environment* **53**(0), 119 – 127 (2012).

[4] Gavrilakis, S. *Journal of Fluid Mechanics* **244**, 101–129 (1992).

[5] Zhang, H., Trias, F., Tan, Y., Y.Sheng, and Oliva, A. *23rd International Conference on Parallel Computational Fluid Dynamics, Barcelona* , 1–5 (2011).

[6] Trias, F. X., Gorobets, A., Zhang, H., and Oliva, A. *Procedia Engineering* **61**(0), 179 – 184 (2013).

[7] Yao, J. and Fairweather, M. *Physics of Fluids* **22**(3), 03330301–15 (2010).

[8] Adams, J., Fairweather, M., and Yao, J. *Computers and Chemical Engineering* **35**(5), 893 – 900 (2011).

[9] Tanaka, T. and Tsuji, Y. *ASME/FED Gas-Solid flow* **121**, 123–128 (1991).

[10] Cundall, P. *In: Muller led, ed. Proc Symp Int Soc Rock Mechanics, Rotterdam: Balkama A A* **1**, 8–12 (1971).

[11] Yue, X., Zhang, H., Luo, C., Shu, S., and Feng, C. In *Parallel Computational Fluid Dynamics*, 149–159. Springer, (2014).

[12] Cao, G., Zhang, H., Tan, Y., Wang, J., Deng, R., Xiao, X., and Wu, B. *Procedia Engineering* (2014).

[13] Xiao, X., Tan, Y., Zhang, H., Jiang, S., Wang, J., Deng, R., Cao, G., and Wu, B. *Procedia Engineering* (2014).

[14] Zhang, H., Tan, Y., and Li, M. *International Conference on Computer Science and Software Engineering* **3**, 31–34 (2008).

[15] Tan, Y., Zhang, H., Yang, D., Jiang, S., Song, J., and Sheng, Y. *Tribology International* **46**(1), 137 – 144 (2012).

[16] Zhang, H., Tan, Y., Yang, D., Trias, F. X., Jiang, S., Sheng, Y., and Oliva, A. *Powder Technology* **217**, 467 – 476 (2012).

[17] Verstappen, R. W. C. P. and Veldman, A. E. P. *Journal of Computational Physics* **187**, 343–368 (2003).

[18] Trias, F. X. and Lehmkuhl, O. *Numerical Heat Transfer, Part B: Fundamentals* **60**(2), 116–134 (2011).

[19] Trias, F. X., Soria, M., Oliva, A., and Pérez-Segarra, C. D. *Journal of Fluid Mechanics* **586**, 259–293 (2007).

[20] Johnson, K. *Cambridge University Press, Cambridge* (1985).

[21] Mindlin, R. and Deresiewicz, H. *Journal of Applied Mechanics* **20**, 327–344 (1953).

[22] Zhang, H., Tan, Y., Shu, S., Niu, X., Trias, F. X., Yang, D., Li, H., and Sheng, Y. *Computers & Fluids* **94**(0), 37 – 48 (2014).

[23] Uhlmann, M., Pinelli, A., Kawahara, G., and Sekimoto, A. *Journal of Fluid Mechanics* **588**, 153–162 (2007).

[24] Raiesi, H., Piomelli, U., and Pollard, A. *Journal of Fluids Engineering* **133**(2) (2011).